

# Revealing a multiplex brain network through the analysis of recurrences

Cite as: Chaos **30**, 121108 (2020); <https://doi.org/10.1063/5.0028053>

Submitted: 02 September 2020 . Accepted: 30 November 2020 . Published Online: 21 December 2020

 Nikita Frolov,  Vladimir Maksimenko, and  Alexander Hramov



View Online




Export Citation




CrossMark





Sign up for topic alerts

New articles delivered to your inbox



# Revealing a multiplex brain network through the analysis of recurrences

Cite as: Chaos 30, 121108 (2020); doi: 10.1063/5.0028053

Submitted: 2 September 2020 · Accepted: 30 November 2020 ·

Published Online: 21 December 2020



View Online



Export Citation



CrossMark

Nikita Frolov,<sup>1,a)</sup> Vladimir Maksimenko,<sup>1</sup> and Alexander Hramov<sup>1,2</sup>

## AFFILIATIONS

<sup>1</sup>Neuroscience and Cognitive Technology Laboratory, Center for Technologies in Robotics and Mechatronics Components, Innopolis University, 420500 Innopolis, The Republic of Tatarstan, Russia

<sup>2</sup>Lobachevsky University, 23 Gagarina Avenue, 603950 Nizhny Novgorod, Russia

<sup>a)</sup>Author to whom correspondence should be addressed: [n.frolov@innopolis.ru](mailto:n.frolov@innopolis.ru)

## ABSTRACT

A multilayer approach has recently received particular attention in network neuroscience as a suitable model to describe brain dynamics by adjusting its activity in different frequency bands, time scales, modalities, or ages to different layers of a multiplex graph. In this paper, we demonstrate an approach to a frequency-based multilayer functional network constructed from nonstationary multivariate data by analyzing recurrences in application to electroencephalography. Using the recurrence-based index of synchronization, we construct intralayer (within-frequency) and interlayer (cross-frequency) graph edges to model the evolution of a whole-head functional connectivity network during a prolonged stimuli classification task. We demonstrate that the graph edges' weights increase during the experiment and negatively correlate with the response time. We also show that while high-frequency activity evolves toward synchronization of remote local areas, low-frequency connectivity tends to establish large-scale coupling between them.

Published under license by AIP Publishing. <https://doi.org/10.1063/5.0028053>

Complex network theory provides appropriate graph-theoretical tools and models to describe brain functioning from an integrative perspective. Specifically, previous studies report the multiplex network's relevance in consideration of the functionally dissociated neuronal interactions by adjusting connectivity within frequency bands of interest to the different layers of the graph. Simultaneously, the graph's interlayer connections might be defined by a local cross-frequency coupling (CFC), establishing coordination of within-frequency synchronized neuronal populations. Combining both types of coupling, multilayer networks represent a suitable model for exploring large-scale neuronal interactions. To properly construct graph edges from magneto- or electroencephalography (M/EEG) recordings based on the estimation of phase synchronization (PS), one should apply advanced methods for nonlinear time-series analysis robust against the nonstationarity and poor signal-to-noise ratio of these signals. Here, we demonstrate an approach to multilayer functional networks from nonstationary multivariate data by analyzing recurrences in application to electroencephalography (EEG). We employ this method to reveal the evolution of functional

cortical connectivity in the course of a prolonged cognitive task. Using a multilayer analysis, we demonstrate the growth of the graph edges' weights during the experiment and their negative correlation with the response time. Besides, we establish that while high-frequency activity coordinates remote local areas' synchronization, low-frequency connectivity tends to establish large-scale coupling between them.

## I. INTRODUCTION

Brain activity captured by magneto- and electroencephalography (M/EEG) represents a combination of broadband neuronal oscillations, or brain rhythms.<sup>1</sup> Different rhythms underlie functionally dissociated brain activity and their interaction forms a core of cognition.<sup>2</sup>

Particularly, synchronization of slow theta (4–8 Hz) oscillations mediates large-scale neuronal interactions in human memory and sensorimotor integration,<sup>3–6</sup> whereas brain-wide alpha (8–12 Hz) and beta (15–30 Hz) coupling stands behind the

top-down communication, sensory processing, and perceptual decision-making.<sup>7–10</sup>

At the same time, interaction between neuronal oscillations in different frequency bands, i.e., a cross-frequency coupling (CFC), determines the established spike-timing relationships and, thus, coordinates the activity of within-frequency synchronized neuronal ensembles.<sup>11–13</sup> Recent studies report the vital role of CFC in visual working memory and attention tasks.<sup>11,14</sup>

Thus, both within- and cross-frequency connections play important roles in coordination of neuronal processing. Considering these processes from an integrative perspective, modern neuroscience actively employs network theory that provides a set of relevant graph-theoretical tools to describe brain functioning during task-related activity and at rest.<sup>15,16</sup> In this context, a multilayer network, where each layer is adjusted to within-frequency synchronized networks and CFC is defined by the multiplex connections, is a suitable construct for modeling neuronal communication.<sup>17–23</sup>

Constructing edges of such a functional multilayer graph from multichannel M/EEG data is usually based on the quantification of phase synchronization (PS)—a cornerstone mechanism of establishing spike-time relationships between neuronal ensembles.<sup>24,25</sup> Traditionally, PS is measured in terms of 1:1 phase-locking<sup>26</sup> in the case of within-frequency coupling and *n:m* phase-locking in the case of CFC.<sup>27</sup> At the same time, M/EEG recordings represent noisy non-stationary data, especially at high frequencies, where the signal-to-noise ratio is naturally poor, and thus a correct definition of phase may be problematic, since stronger noise causes undesirable phase slips.<sup>27,28</sup> Also, in the case of CFC, phase-locking measures are sensitive to the definition of main frequencies of the interacting brain rhythms and the ratio between them.

A potential way to overcome these limitations is to use recurrence quantification analysis (RQA)—a powerful toolbox for non-linear time-series processing, which estimates the probability of a system to visit its previous states, i.e., to recur.<sup>29,30</sup> In Ref. 31, Romano *et al.* introduced the recurrence-based measures to quantify phase and generalized synchronization in a pair of interacting systems through the analysis of their joint recurrences. Further, a bulk of studies has shown the applicability of the recurrence-based measures of synchronization to the within-frequency analysis of integrative processes in the brain.<sup>32–37</sup> However, a possibility to reveal cross-frequency synchrony has not been demonstrated so far.

In this work, we have applied the recurrence-based analysis to construct the edges of a multiplex brain graph from the multichannel EEG. We show that the recurrence-based approach is essentially suitable for a CFC problem being compared with the traditionally applied phase-locking value (PLV). We also emphasize that the analysis of recurrences gives clearly interpreted results in terms of cross-frequency modulation. In the framework of the multilayer approach, we have modeled the evolution of a prestimulus functional connectivity in the course of a prolonged cognitive task. We have adjusted each layer to the cortical connectivity within specific frequency bands—theta (4–8 Hz), alpha (8–12 Hz), and beta (15–30 Hz)—whereas interlayer links have defined the local cross-frequency synchrony. We reveal the properties of functional connectivity from a multilayer perspective, which, we suggest, underlie the improvement of behavioral performance.

## II. METHODS

### A. Connectivity analysis

In this work, we carried out sensor-level functional connectivity analysis following the recurrence-based approach to detect synchronization for a non-stationary time-series developed by Romano *et al.*<sup>31</sup> Functional connectivity was estimated during the 1 s prestimulus period, i.e., in a time frame [−1, 0] s, where time 0 corresponded to a stimulus presentation.

#### 1. Recurrence analysis

Given two EEG signals  $x(t)$  and  $y(t)$ , we applied Takens' embedding theorem<sup>38</sup> with time delays  $\tau^{x,y}$  and embedding dimensions  $d^{x,y}$  to construct the corresponding trajectories  $\{\mathbf{x}_i\}_{i=1}^N$  and  $\{\mathbf{y}_i\}_{i=1}^N$ .

Recurrence plots (RPs) of these trajectories and their joint recurrence plot (JRP) were defined as the matrices,

$$\begin{aligned} \mathbf{R}_{ij}^x &= \Theta(\epsilon^x - |\mathbf{x}_i - \mathbf{x}_j|), \\ \mathbf{R}_{ij}^y &= \Theta(\epsilon^y - |\mathbf{y}_i - \mathbf{y}_j|), \\ \mathbf{JR}_{ij} &= \mathbf{R}_{ij}^x \mathbf{R}_{ij}^y, \end{aligned} \quad (1)$$

where  $\epsilon^{x,y}$  were the fixed thresholds and  $\Theta(\bullet)$  was a Heaviside function. As shown in Ref. 31, analyzing joint recurrences it is more appropriate to use a fixed number of the nearest neighbors  $N_N$ <sup>39</sup> to compute recurrence matrices  $\mathbf{R}^{x,y}$  instead of the fixed threshold approach. In this case, the average probability of recurrence over the considered time interval for the trajectory  $\mathbf{x}$  was  $RR^x = N_N/N$  (analogously for the trajectory  $\mathbf{y}$ ). Since the ratio  $N_N/N$  was chosen equal for both trajectories, let us redefine it as  $N_N/N = RR$  so that  $RR^x = RR^y = RR$ . At the same time, the average joint probability of the recurrence over the time was defined as

$$JRR = \frac{1}{N^2} \sum_{i,j=1}^N \mathbf{JR}_{ij}. \quad (2)$$

If the trajectories  $\mathbf{x}_i$  and  $\mathbf{y}_i$  were independent, then the averaged joint probability of recurrence was  $JRR = RR^x RR^y$ , whereas the dependent trajectories implied  $JRR \neq RR^x RR^y$ . Thus, the index of synchronization, defined as

$$S_{xy} = \frac{JRR}{RR}, \quad (3)$$

lies between  $RR$  (independent processes) and 1 (generalized synchronization).

Previous studies reported that the recurrence-based approach was suitable in inference of dependencies in EEG data, particularly considering event-related potentials in the oddball paradigm,<sup>32</sup> functional connectivity associated with mental fatigue,<sup>35</sup> and cortical interactions during the perceptual decision-making task.<sup>37</sup> Here, we demonstrate that besides the connectivity analysis within a specific frequency band, the recurrence-based index of synchronization is essentially applicable for the analysis of *cross-frequency synchronization*. Notably, the advance of the above described recurrence-based method does not require any modification or parameter tuning.

Also, the recurrence-based index of synchronization  $S_{xy}$  demonstrated the robustness against the parameters of the RPs calculation (see Sec. III).

RQA was performed using the *pyunicorn* package for Python.<sup>40</sup>

## 2. Phase-locking value

To verify the efficiency of the recurrence-based approach in the context of CFC problem, we used the phase-locking value (PLV)—a traditional measure of PS.<sup>11,13,26,27</sup> Given a pair of slow and fast components of signal  $x(t)$  having characteristic frequencies  $f_{slow}$  and  $f_{fast}$ , we defined a PLV measure as

$$PLV_m^x = \frac{1}{N} \left| \sum_{i=1}^N e^{i(\phi_{slow,i}^x - m\phi_{fast,i}^x)} \right|, \quad m = \frac{f_{slow}}{f_{fast}}, \quad (4)$$

where  $\phi_{slow}^x$  and  $\phi_{fast}^x$  are the instantaneous phases extracted from the slow and fast components of signal  $x(t)$  via Hilbert transform. For further simplicity, we redefine the cross-frequency phase difference as  $\Delta\phi_{m,i}^x = \phi_{slow,i}^x - m\phi_{fast,i}^x$ .

## B. Multiplex graph

Calculating a recurrence-based index of synchronization  $S_{xy}$  for all possible edges of the multiplex graph for each  $k$ th EEG epoch of the  $n$ th subject, we filled the resulting weight matrices  $\mathbf{W}_{xy}^{k,n,(Begin,End)}$  sized  $3N_s \times 3N_s$ , where superscripts “Begin” and “End” corresponded to the beginning and ending of task, respectively. These matrices represented a weighted three-layer multiplex brain graphs, which described both within- and cross-frequency neuronal interactions in the frequency bands of interest: theta (4–8 Hz), alpha (8–12 Hz), and beta (15–30 Hz).

Separate layers of the multilayer graph were represented by the non-overlapping  $N_s \times N_s$  sub-matrices lying along the main diagonal and defined the sensor-to-sensor within-frequency (intralayer) functional connectivity. Intralayer functional connectivity did not take into account self-loops; thus, these sub-matrices had zero elements on their main diagonals. The remaining non-overlapping  $N_s \times N_s$  sub-matrices defined the local CFC (interlayer multiplex connections). These sub-matrices had non-zero elements only on their main diagonals. The non-zero elements of  $\mathbf{W}_{xy}^{k,n,(Begin,End)}$  quantified the within- and cross-frequency coupling strength via a recurrence-based index of synchronization  $\mathbf{W}_{xy}^{k,n,(Begin,End)} = S_{xy}^{k,n,(Begin,End)}$ .

Finally, to model brain connectivity reconfiguration from beginning to ending of the experiment, we evaluated the structure of a functional multilayer graph composed of the connections exhibiting significant changes via a within-group non-parametric statistical analysis. For this purpose, we considered matrices  $\mathbf{W}_{xy}^{n,C}$ , i.e., weight matrices averaged across the epochs. First, we carried a pairwise comparison of each multilayer graph’s edge between beginning and ending conditions “End” and “Begin” via one-tailed paired  $t$ -test ( $dF = 19$ ,  $t_{critical} = \pm 2.093$ ). Further, we applied cluster-based Network-Based Statistic (NBS) approach<sup>41</sup> to control the family-wise error rate with  $r = 1000$  random permutations and the significance level of  $p_{cluster} < 0.05$ . The identified cluster of the multilayer graph

described the transformation of a prestimulus brain functional connectivity and was stored as the adjacency matrix  $\mathbf{A}_{xy}$ .

## III. RESULTS AND DISCUSSION

We have conducted the EEG experiment aimed at revealing changes in the human’s behavior and brain activity during a prolonged cognitive task, which involved perceptual decision-making and maintenance of visual attention. Specifically, the task has required the participants ( $P = 20$  subjects, 9 females, aged 26–35) to quickly perceive successively presented bistable visual stimuli and report one of their possible interpretations right after the presentation. In this study, we have used the ambiguous image of Necker cube as a bistable visual stimulus, whose contrast of the inner edges defines both cube’s orientation and ambiguity [Fig. 1(a)]. The conducted prolonged experimental session lasts for approximately 40 min and requires classification of 400 visual stimuli [Fig. 1(b)]. See the [supplementary material](#) for a detailed information about the experimental paradigm and EEG data acquisition.

First, we have evaluated the effect of subject’s performance in terms of their response time [RT, Fig. 1(c)] taking into account factors of Time (“Begin” and “End” conditions) and stimuli Ambiguity (high-ambiguity “HA” and low-ambiguity “LA”). Repeated measures ANOVA has revealed a significant main effect of both factors [Time:  $F(1, 19) = 18.65$ ,  $p < 0.001$ ; Ambiguity:  $F(1, 19) = 50.48$ ,  $p < 0.001$ ]. *Post hoc* comparison via paired  $t$ -test indicated that RT at the beginning of the experiment ( $1.146 \pm 0.390$  s, mean  $\pm$  SD) is significantly higher than RT at the end of the experiment ( $0.957 \pm 0.270$  s, mean  $\pm$  SD). Regarding the Ambiguity, RT on HA stimuli ( $1.175 \pm 0.327$  s, mean  $\pm$  SD) is significantly higher than RT on LA stimuli ( $0.928 \pm 0.325$  s, mean  $\pm$  SD). In turn, the interaction between these factors has been insignificant [ $F(1, 19) = 1.08$ ,  $p = 0.312$ ]. We can interpret these results as a meaning that the subjects increase their performance in terms of reducing their RT from the beginning to the end of the experimental session irrespective of the stimuli ambiguity. For detailed Repeated measures ANOVA summary, please see Tables I and II in the [supplementary material](#).

The considered cognitive task implies response to the repeatedly presented visual stimuli with similar morphological properties. The neuroimaging studies have suggested that the neuronal adaptation causes the activation of the local neuronal populations in the sensory area prior to stimulus onset to reduce cognitive demands and increase behavioral response.<sup>42–44</sup> We expect the similar effect on the integrative level, i.e., as an emergence of a prestimulus functional connectivity pattern.

We have addressed this problem by modeling the underlying neuronal interactions as a multiplex graph, which has combined both within-frequency (intralayer) and local cross-frequency (interlayer) coupling connections. The ability to reveal synchrony between the brain signals filtered in the same frequency band through the analysis of recurrences is undoubted and has been demonstrated in the bulk of literature.<sup>32–37</sup> However, here we demonstrate that the recurrence-based approach also perfectly suites the CFC problem. Figure 2 gives an exemplary illustration of this approach and shows the clarity of its interpretation. Figure 2(a) presents fast beta-band (middle) and slow theta-band (bottom) oscillations extracted from a single 1 s epoch of the broadband prestimulus electrical cortical

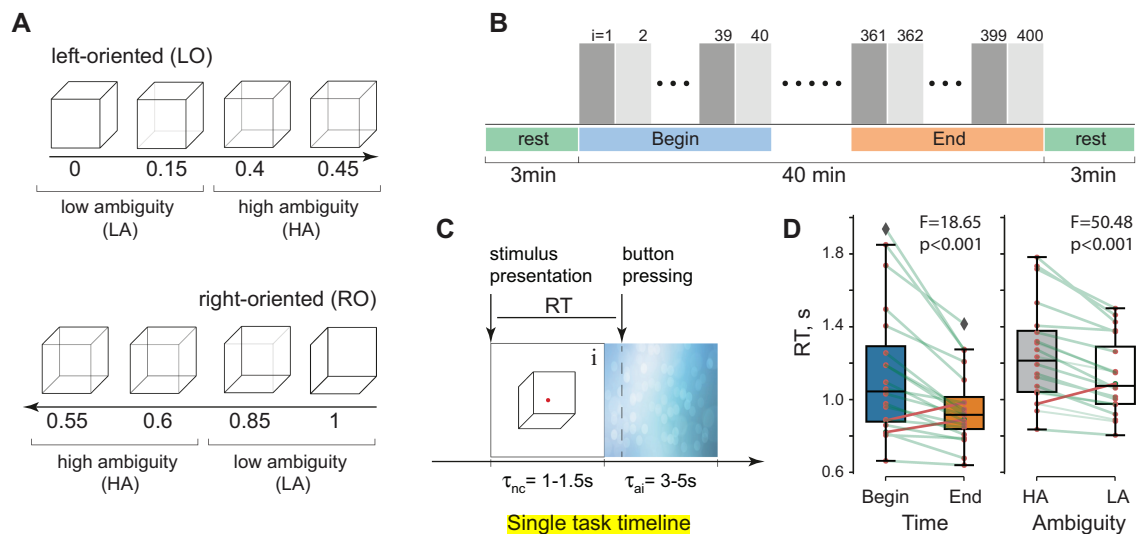


**FIG. 1.** Experimental paradigm and behavioral results. (a) The set of presented ambiguous Necker cube images: left-oriented (top panel) and right-oriented (bottom panel). The ambiguity of visual stimuli is indicated at the bottom of each panel. (b) The timeline of experimental session, which included the eyes open rest state recording (green areas, about 3 min before and after the prolonged cognitive task) and successive presentation of ambiguous visual stimuli (each stimulus presentation is illustrated as a gray block). "Begin" and "End" conditions are highlighted with blue and orange areas, respectively. (c) The timeline of the  $i$ th visual stimulus presentation. (d) Comparison of the mean response time (RT) between subjects via Repeated measures ANOVA taking into account the factors of Time (left panel) and stimuli Ambiguity (right panel). In the paired plots, the transparent green lines indicate subjects demonstrating the effect and the bold red lines highlight subjects who do not.

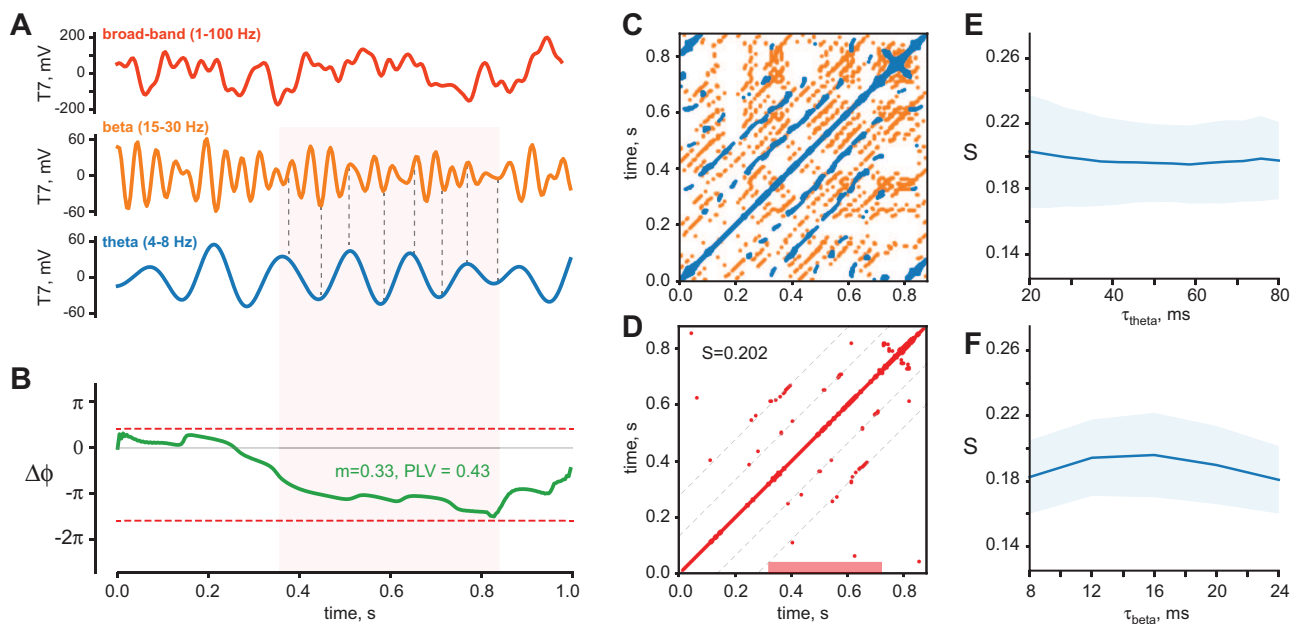


**FIG. 2.** Exemplary illustration of the single-trial CFC inference via Joint Recurrence Analysis. (a) Broadband (1–100 Hz, red curve), fast beta-band (15–30 Hz, orange curve), and slow theta-band (4–8 Hz, blue curve) oscillations during a prestimulus brain activity recorded by T7 EEG sensor. (b) CF phase difference calculated for  $m = 1 : 3 \approx 0.33$ . Shading highlights a CF phase synchronization area. (c) Visualization of the recurrence matrices  $R_{ij}$  of the fast (beta-band) and slow (theta-band) trajectories reconstructed from signals presented in (a). (d) Visualization of the joint recurrence matrix  $JR_{ij}$  of the beta- and theta-band trajectories presented in (c). Dashed diagonal lines correspond to a single and double period of slow (theta-band) oscillations. Shading highlights the area of the CFC defined by the presence of the non-zero elements lying on the dashed diagonal lines. The dependencies of recurrence-based index of synchronization  $S$  on the embedding delays  $\tau_{theta}$  (e) and  $\tau_{beta}$  (f). The dependencies are presented as mean  $\pm$  SD across the subjects.



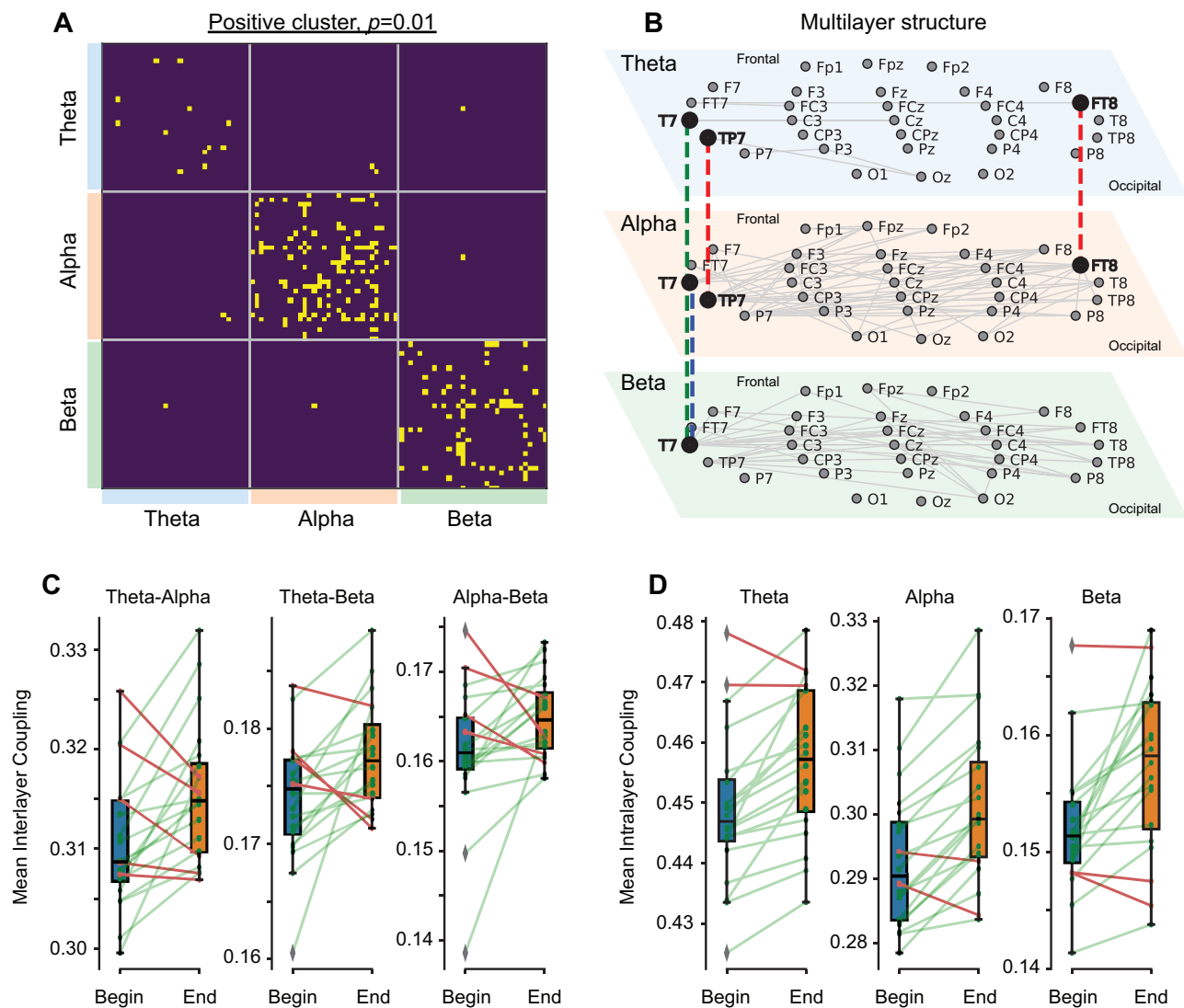


**FIG. 3.** Revealing a multiplex graph. (a) The adjacency matrix  $A_{xy}$  representing functional connections exhibiting positive significant changes of the recurrence-based index synchronization between experimental conditions “End” vs “Begin” ( $p = 0.01$  via NBS). (b) The structure of the multilayer functional network stored in the adjacency matrix  $A_{xy}$ . Here, thin gray lines show the intralayer links, and dashed colored lines highlight interlayer links: theta-beta (green), theta-alpha (red), and alpha-beta (blue). Comparison of the mean interlayer (c) and intralayer (d) coupling weights between subjects via Repeated measures ANOVA taking into account the factors of Time and Frequency Band. All paired plots reflect a significant difference between the “Begin” and “End” conditions with  $p < 0.001$ . In the paired plots, the transparent green lines indicate subjects demonstrating the effect and the bold red lines highlight subjects who do not.

activity (top) recorded at the temporal EEG sensor T7. Results of the cross-frequency synchrony analysis via a traditional PLV measure are presented in Fig. 2(b). Following Tass *et al.*,<sup>27</sup> we have defined  $m$  as a ratio of two integers  $1 : 3 \approx 0.33$  and achieved  $PLV = 0.43$  [green curve in Fig. 2(b)]. The corresponding phase difference  $\Delta\phi(t)$  lies within a  $2\pi$  interval bounded by red dashed lines in Fig. 2(b) and has a plateau within an approximate interval  $[0.4, 0.8]$ s.

At the same time, the cross-frequency coupling in terms of recurrences should be understood as an increased probability of the

fast oscillation’s trajectory visiting its previous states if modulated by a slow electrical activity. Accordingly, CFC should be detected in JRP by emergent dots lying on the diagonal lines parallel to the main diagonal and spaced from it at a distance multiple of the characteristic period of slow oscillations.

To reconstruct the trajectories of neuronal activity in the frequency bands of interest, we used embedding delays equal to one third of the characteristic oscillation period:  $\tau_{\theta} = 52$  ms (13 data points),  $\tau_{\alpha} = 32$  ms (8 data points), and  $\tau_{\beta} = 16$  ms (4 data

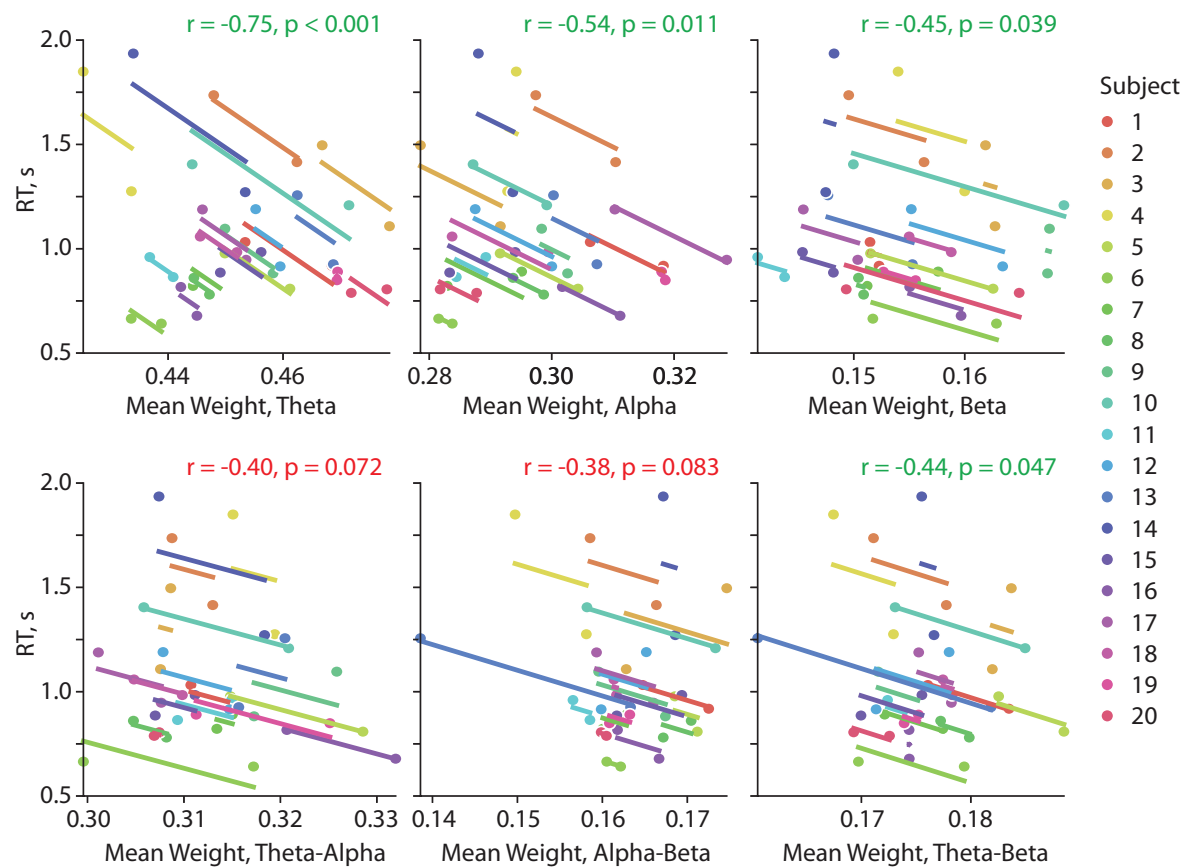


**FIG. 4.** Repeated measures correlation (rmcorr) between the weights of graph edges and the RT. Rmcorr plots illustrating the correlation between the mean intralayer (upper panel) and interlayer (bottom panel) coupling weights and the RT. Upper panel: theta layer (left plot), alpha layer (middle plot), and beta layer (right plot). Bottom panel: theta-alpha coupling (left plot), alpha-beta coupling (middle plot), and theta-beta coupling (right plot). Rmcorr coefficients  $r$  and corresponding  $p$ -values are presented in each plot.

points). Embedding dimension  $d = 3$  was chosen equally for all brain considered rhythms. Figure 2(c) shows the RPs constructed for the fast (orange dots) and slow (blue dots) neuronal oscillations, and their JRP is presented in Fig. 2(d). It is seen that the joint recurrence dots appear in JRP at the diagonal lines spaced from the main diagonal at a single and double period of slow neuronal activity and manifest a pronounced CSF between 0.4 and 0.7 s, which nicely coincides with the estimation given above by PLV. In this case, the recurrence-based index of synchronization  $S$  reaches the value 0.2, which exceeds the non-independence level of  $RR = 0.05$  and, therefore, indicates the dependence between the considered time-series. Importantly, the value of  $S$  is robust against the parameters of the time-series embedding: the dependencies of  $S$  on embedding delays  $\tau_{theta}$  and  $\tau_{beta}$  are presented in Figs. 2(e) and 2(f), respectively. One can see that variation in delay in a fairly wide range does not crucially influence the value of the synchronization index  $S$ . However, our empirical findings suggest that one third of a characteristic oscillation period is an optimal choice for embedding delay in the case of EEG signals.

Above, we have confirmed the adequacy of the recurrence-based index of synchronization in quantification of the local CFC from non-stationary EEG data. Next, using this measure we have filled the matrices  $\mathbf{W}_{xy}^{k,n,[Begin,End]}$  and restored a multiplex graph to model the changes in a prestimulus cortical connectivity. A within-subject NBS has revealed a positive prestimulus connectivity cluster ( $p = 0.01$ ), i.e., a multilayer sub-graph, whose edges exhibited a significant coupling increase from the beginning to ending of the prolonged task. Corresponding adjacency matrix  $\mathbf{A}_{xy}$  and network structure are shown in Figs. 3(a) and 3(b). Further, we discuss the evolution of the functional connectivity in terms of a multilayer network treatment.

First, the recurrence-based approach has revealed several intensifying interlayer links supporting the local CFC in remote brain regions—frontal-temporal and parietal-temporal areas. Specifically, an increased theta-alpha coupling has been found in the frontal-temporal sensor FT8 and temporal-parietal sensor TP7 and theta-beta coupling has been observed in the temporal sensor T7 that has also demonstrated growing alpha-beta coupling. The interaction

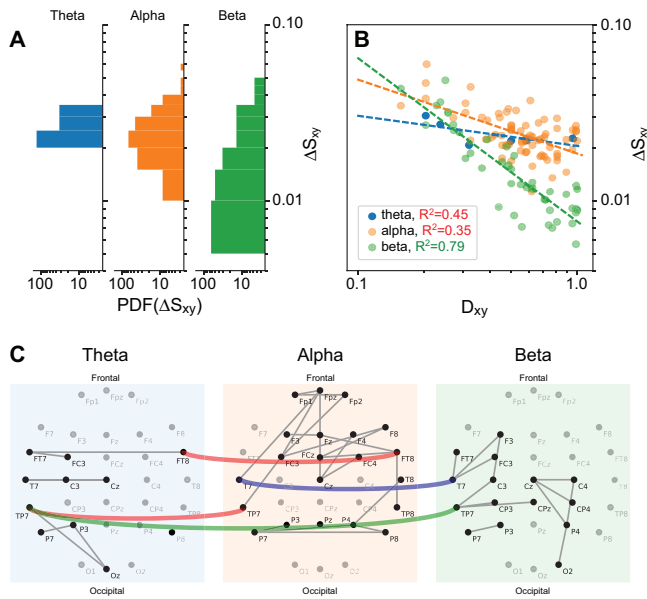


**FIG. 5.** Properties of the intralayer coupling. (a) Probability density functions (PDFs) of the intralayer coupling weights increase  $\Delta S_{xy}$  presented on a log-log scale. (b) Dependencies of the intralayer coupling weights increase  $\Delta S_{xy}$  on the normalized nodes distance  $D_{xy}$  in theta (blue circles), alpha (orange circles), and beta (green circles) layers presented on a log-log scale. Dashed colored lines indicate the corresponding power law approximations. The values of  $R^2$  are presented in the legend. (c) The structure of the multilayer functional network with excluding weak intralayer links in alpha and beta layers, i.e., the 70th percentile of their PDFs from (a).

between the layers through the local CFC has been characterized by the different values of the mean interlayer coupling [ $p < 0.001$  via Repeated measures ANOVA, Fig. 3(c) and Tables III and IV in the [supplementary material](#)]. The strongest interaction has been found between the theta and alpha layers, whereas mean theta-beta and alpha-beta coupling have considerably exceeded a non-independence threshold.

Second, we have found that the mean coupling strength of the intralayer functional connectivity varied from layer to layer [ $p < 0.001$  via Repeated Measures ANOVA, see Fig. 3(d) and Tables V and VI in the [supplementary material](#)]. On the one hand, a signal-to-noise ratio decays with increasing frequency, which worsens the estimation of phase. One might also suppose that phase-locking at higher frequency bands is possible for much shorter time scales than at low-frequency bands. These factors naturally reduce the level of estimated synchronization measure from low theta to high beta band. On the other hand, this result might emphasize that stronger synchrony of the low-frequency oscillations contributes more to a brain-wide communication than the high-frequency activity.

We analyzed the correlation between the RT and the weights of the uncovered graph edges. With this aim, we have applied Repeated measures correlation (rmcorr) to explore the relationship between the two considered variables, while controlling the between-participants variance.<sup>45</sup> Figure 4 demonstrates that the RT

is negatively correlated with mean intralayer weights of all layers of the uncovered multiplex graph, whereas the highest correlation within theta layer. Regarding the interlayer coupling, only theta-beta weights negatively correlate with RT (Table VII in the [supplementary material](#)).

The bulk of literature reports an essential role of neural activity in the considered frequency bands for visual stimuli processing. Neural activity in the beta-frequency band plays a vital role in ambiguous information processing.<sup>10</sup> According to Engel and Fries,<sup>46</sup> processing an ambiguous stimulus involves a strong endogenous, top-down component associated with the high beta-band activity. The neural activity in the alpha-band also determines performance in the visual perception task.<sup>47</sup> In particular, it subserves inhibition of the irrelevant sensory information, which is also crucial for effective processing.<sup>48</sup> The prestimulus spectral power and functional connectivity in alpha- and beta-bands characterize attention state and also affect ongoing stimulus processing.<sup>37</sup> Activity in the theta-band contributes to the functional interaction between the different cortical regions. Synchronization of theta-band activity in the sensory and frontal regions increases during sensory-processing tasks requiring attention and working memory.<sup>49</sup> Functional interactions in theta-band may also contribute to integrating external sensory information with internal expectations, facilitating ambiguous stimuli processing. Neuronal activity in temporal areas appears to be involved in the high-level visual processing of complex stimuli. This area contains higher levels of the ventral stream of visual processing associated with the final representation of objects.

Finally, we have uncovered the difference in the intralayer topological properties of the functional multiplex network. We have considered the distributions of intralayer coupling weights  $\Delta S_{xy}$  corresponding to the edges of the uncovered positive network cluster (Fig. 5). Here,  $\Delta S_{xy}$  defines the change of intralayer coupling weight in a pair of EEG sensors  $x$  and  $y$  between the ending and beginning of the experiment, i.e.,  $\Delta S_{xy} = \langle S_{xy}^{End} \rangle - \langle S_{xy}^{Begin} \rangle$  and  $\langle \bullet \rangle$  is an averaging across subjects. Figure 5(a) shows the probability density functions (PDFs) of  $\Delta S_{xy}$  in different layers of the reconstructed multilayer graph. It is seen that the low-frequency theta-band layer is composed of a few sparse connections and characterized by a uniformly strong increase of coupling ( $\Delta S_{xy} = 0.02/0.035$ , blue bins). PDFs of the other layers become more skewed to the lower values of  $\Delta S_{xy}$  with increasing frequency of the band. At the same time, both alpha and beta layers are characterized by the long-tailed PDFs implying the emergence of rather strongly intensified edges. Considering the dependence of the edges' weights  $\Delta S_{xy}$  on the normalized distance  $D_{xy}$  between EEG sensors  $x$  and  $y$ , we have found that  $\Delta S_{xy}$  decreased with  $D_{xy}$  for alpha and beta layers [Fig. 5(b)]. At the same time, coupling weights of the beta layer decay much stronger at high distances ( $D_{xy} > 0.5$ ) than in both theta and alpha layers.

Fitting the layer's weight distribution by the power law  $\Delta S_{xy} \sim D_{xy}^{\beta}$ , we have found a nice agreement in beta layer ( $\beta = -0.93$ ,  $R^2 = 0.79$ ). Following Bak *et al.*,<sup>50</sup> this dependence, roughly equal to  $D_{xy}^{-1}$ , reflects the route to a beta-band neuronal self-organized criticality, or spatial self-similarity.<sup>51</sup> It means that during a prolonged task, prestimulus beta-band connectivity evolves toward a critical state, where local neuronal populations are strongly coupled



through fast oscillations to perform neuronal processing, but weakly coupled between each other. In contrast, slow theta ( $\beta = -0.17$ ,  $R^2 = 0.45$ ) and alpha ( $\beta = -0.42$ ,  $R^2 = 0.35$ ) layers do not obey the power law and exhibit stronger coupling increase at the large distances ( $D > 0.5$ ). Excluding weakly coupled edges, we again construct the resulting multilayer graph in Fig. 5(c). Indeed, alpha and beta layers represent two spatially dissociated networks. At the same time, due to the emergence of several large-scale links in theta layer along with interlayer edges connecting the most influential nodes, we suppose that slow theta-band oscillations support coordination of alpha and beta networks via establishing proper phase relations between remote locally synchronized groups.

#### IV. CONCLUSION

To summarize, we have demonstrated an approach to frequency-based multilayer brain networks through the recurrence analysis of multichannel EEG recordings. Specifically, we have considered a multiplex model composed of both within-frequency connections (intralayer edges) and cross-frequency coupling (multiplex interlayer edges). We have shown that the recurrence-based synchronization index is a well-suited tool for inferring both mentioned types of neuronal interactions, being robust against time-series embedding parameters and EEG signal's non-stationarity.

Using this approach, we have addressed the reconfiguration of whole-head prestimulus functional connectivity during a prolonged cognitive task. Analyzing the evolution of integrative brain activity from a multilayer perspective, we have inferred that shortening response time during the visual stimuli classification task is accompanied by enhanced prestimulus functional interactions in the whole-head functional connectivity network in theta, alpha, and beta frequency bands. We have also found that increased prestimulus theta-beta coupling at the left temporal sensors positively correlates with the response time. We suppose that strong prestimulus theta-beta coupling in the high-level processing areas manifests increased reliance of the ongoing stimulus interpretation on the internal processes such as working memory and expectations. The latter may decrease processing demands and increases behavioral performance.

Besides, we have demonstrated that in the course of a prolonged task, prestimulus high-frequency activity tends to self-organize in sparse locally coupled ensembles. In contrast, slow neuronal oscillations contribute to a large-scale connection between these populations. We suggest that the revealed mechanism of brain connectivity self-organization is related to a preactivation of specific functional links relevant to upcoming task-related activity and aims to decrease cognitive demands and enhance behavioral performance.

We expect that the developed recurrence-based approach might be useful for a deeper understanding of neuronal communication mechanisms and contributes to developing graph-theoretical methods for modern neuroscience.

#### SUPPLEMENTARY MATERIAL

See the supplementary material for a detailed information about the experimental paradigm and data acquisition.

#### ACKNOWLEDGMENTS

This work has been supported by the Russian Foundation for Basic Research (Grant No. 19-52-45026) and by the Council for Grants of the President of the Russian Federation (Grant Nos. MK-2080.2020.2 and MK-1760.2020.2). A.E.H. also acknowledges the Lobachevsky University competitiveness program in the frame of 5-100 Russian Academic Excellence Project.

The authors gratefully acknowledge the anonymous reviewer for the valuable remarks and suggestions.

#### DATA AVAILABILITY

The data that support the findings of this study are openly available in the Figshare repository at <https://doi.org/10.6084/m9.figshare.12301181>, Ref. 52.

#### REFERENCES

- G. Buzsaki, *Rhythms of the Brain* (Oxford University Press, 2006).
- P. Fries, *Neuron* **88**, 220 (2015).
- M. W. Jones and M. A. Wilson, *PLoS Biol.* **3**, e402 (2005).
- K. L. Anderson, R. Rajagovindan, G. A. Ghacibek, K. J. Meador, and M. Ding, *Cereb. Cortex* **20**, 1604 (2010).
- L. C. Cruikshank, A. Singhal, M. Hueppelsheuser, and J. B. Caplan, *J. Neurophysiol.* **107**, 65 (2012).
- N. S. Frolov *et al.*, *PLoS One* **15**, e0233942 (2020).
- S. Palva and J. M. Palva, *Front. Psychol.* **2**, 204 (2011).
- A. M. Bastos *et al.*, *Neuron* **85**, 390 (2015).
- C. Palmer, L. Zapparoli, and J. M. Kilner, *Trends. Cogn. Sci. (Regul. Ed.)* **20**, 321 (2016).
- V. A. Maksimenko *et al.*, *Front. Behav. Neurosci.* **14**, 95 (2020).
- F. Siebenhühner, S. H. Wang, J. M. Palva, and S. Palva, *Elife* **5**, e13451 (2016).
- J. M. Palva and S. Palva, *Eur. J. Neurosci.* **48**, 2399 (2018).
- F. Siebenhühner *et al.*, *PLoS Biol.* **18**, e3000685 (2020).
- P. Sauseng, W. Klimesch, W. R. Gruber, and N. Birbaumer, *Neuroimage* **40**, 308 (2008).
- D. Papo, J. M. Buldú, S. Boccaletti, and E. T. Bullmore, *Complex Network Theory and the Brain* (The Royal Society Publishing, 2014).
- D. S. Bassett and O. Sporns, *Nat. Neurosci.* **20**, 353 (2017).
- M. Kivela *et al.*, *J. Complex Networks* **2**, 203 (2014).
- M. J. Brookes *et al.*, *Neuroimage* **132**, 425 (2016).
- M. De Domenico, S. Sasai, and A. Arenas, *Front. Neurosci.* **10**, 326 (2016).
- J. M. Buldú and M. A. Porter, *Network Neurosci.* **2**, 418 (2018).
- M. Vaiana, and S. F. Muldoon, *J. Nonlinear Sci.* **30**, 2147–2169 (2020).
- V. V. Makarov *et al.*, *Phys. Rev. E* **98**, 062413 (2018).
- N. S. Frolov, V. A. Maksimenko, M. V. Khramova, A. N. Pisarchik, and A. E. Hramov, *Eur. Phys. J. Spec. Top.* **228**, 2381 (2019).
- J. Fell and N. Axmacher, *Nat. Rev. Neurosci.* **12**, 105 (2011).
- D. Papo, M. Zanin, and J. Martin Buldú, *Front. Hum. Neurosci.* **8**, 107 (2014).
- J.-P. Lachaux, E. Rodriguez, J. Martinerie, and F. J. Varela, *Hum. Brain Mapp.* **8**, 194 (1999).
- P. Tass *et al.*, *Phys. Rev. Lett.* **81**, 3291 (1998).
- A. Pikovsky, M. Rosenblum, and J. Kurths, *Int. J. Bifurcat. Chaos* **10**, 2291 (2000).
- N. Marwan, M. C. Romano, M. Thiel, and J. Kurths, *Phys. Rep.* **438**, 237 (2007).
- Recurrence Quantification Analysis: Theory and Best Practices*, Springer Series: Understanding Complex Systems, edited by C. L. Webber and N. Marwan, Jr. (Springer International Publishing, Cham, Switzerland, 2015).
- M. C. Romano, M. Thiel, J. Kurths, I. Z. Kiss, and J. Hudson, *Europhys. Lett.* **71**, 466 (2005).
- C. Bandt *et al.*, "Analysis of bivariate coupling by means of recurrence," in *Mathematical Methods in Signal Processing and Digital Image Analysis* (Springer, 2008), pp. 153–182.

- <sup>33</sup>J. L. P. Velazquez, R. G. Erra, R. Wennberg, and L. G. Dominguez, "Correlations of cellular activities in the nervous system: Physiological and methodological considerations," in *Coordinated Activity in the Brain* (Springer, 2009), pp. 1–24.
- <sup>34</sup>Z.-K. Gao *et al.*, *Chaos* **28**, 085713 (2018).
- <sup>35</sup>Y. Yang *et al.*, *IEEE Trans. Syst. Man Cybern. Syst.* (to be published).
- <sup>36</sup>S. Schinkel, G. Zamora-López, O. Dimigen, W. Sommer, and J. Kurths, *J. Neurosci. Methods* **197**, 333 (2011).
- <sup>37</sup>V. A. Maksimenko *et al.*, *Front. Behav. Neurosci.* **13**, 220 (2019).
- <sup>38</sup>F. Takens, "Detecting strange attractors in turbulence," in *Dynamical Systems and Turbulence, Warwick 1980* (Springer, 1981), pp. 366–381.
- <sup>39</sup>J.-P. Eckmann *et al.*, *EPL* **4**, 973 (1987).
- <sup>40</sup>J. F. Donges *et al.*, *Chaos* **25**, 113101 (2015).
- <sup>41</sup>A. Zalesky, A. Fornito, and E. T. Bullmore, *Neuroimage* **53**, 1197 (2010).
- <sup>42</sup>R. Henson and M. Rugg, *Neuropsychologia* **41**, 263 (2003).
- <sup>43</sup>K. Rauss and G. Pourtois, *Front. Psychol.* **4**, 276 (2013).
- <sup>44</sup>N. E. Myers *et al.*, *eLife* **4**, e09000 (2015).
- <sup>45</sup>J. Z. Bakdash and L. R. Marusich, *Front. Psychol.* **8**, 456 (2017).
- <sup>46</sup>A. K. Engel and P. Fries, *Curr. Opin. Neurobiol.* **20**, 156 (2010).
- <sup>47</sup>T. A. De Graaf *et al.*, *PLoS One* **8**, e60035 (2013).
- <sup>48</sup>A. C. Snyder and J. J. Foxe, *J. Neurosci.* **30**, 4024 (2010).
- <sup>49</sup>B. Berger *et al.*, *Nat. Commun.* **10**, 1 (2019).
- <sup>50</sup>P. Bak, C. Tang, and K. Wiesenfeld, *Phys. Rev. A* **38**, 364 (1988).
- <sup>51</sup>G. Buzsáki and A. Draguhn, *Science* **304**, 1926 (2004).
- <sup>52</sup>V. Maksimenko *et al.* (2020). EEG and behavioral data for studying neural adaptation during the prolonged visual stimuli classification task, Figshare Dataset <https://doi.org/10.6084/m9.figshare.12155343.v2>.